Comparison of ultrasound temperature imaging with infrared thermometry during radio frequency ablation

REGULAR PAPER

Comparison of ultrasound temperature imaging with infrared thermometry during radio frequency ablation

Xiaonan Geng[1†], Zhuhuang Zhou[2†], Qiang Li[1], Shuicai Wu[2], Chiao-Yin Wang[3,4],
Hao-Li Liu[5], Ching-Cheng Chuang[6], and Po-Hsiang Tsui[3,7*]

[1]*School of Electronic Information Engineering, Tianjin University, Tianjin 300072, China*
[2]*Biomedical Engineering Center, College of Life Science and Bioengineering, Beijing University of Technology, Beijing 100124, China*
[3]*Department of Medical Imaging and Radiological Sciences, College of Medicine, Chang Gung University, Taoyuan 33302, Taiwan*
[4]*Graduate Institute of Clinical Medical Sciences, College of Medicine, Chang Gung University, Taoyuan 33302, Taiwan*
[5]*Department of Electrical Engineering, Chang Gung University, Taoyuan 33302, Taiwan*
[6]*Institute of Biomedical Engineering, National Chiao Tung University, Hsinchu 30050, Taiwan*
[7]*Institute for Radiological Research, Chang Gung University, Taoyuan 33302, Taiwan*
E-mail: tsuiph@mail.cgu.edu.tw

Radio frequency ablation (RFA) is a widely used alternative modality in the treatment of tumors. During RFA, temperature monitoring is essential to ensure accurate and appropriate thermal dosage. Ultrasound temperature imaging based on the detection of echo time-shift has been demonstrated to have good ability to monitor the temperature distribution. However, no study has proven that the region of ultrasound temperature imaging can correspond well to the practical temperature distribution in the tissue. In this study, we aim to combine ultrasound and infrared systems to clarify the correlation between ultrasound temperature imaging and the practical temperature distribution in a tissue. Five porcine livers ($n = 5$) were ablated using an RFA system and monitored with an ultrasound system to acquire raw backscattered data for temperature imaging. Meanwhile, an infrared imaging system was used to obtain the practical temperature map of the tissue. The results showed that the temperature distribution detected by ultrasound echo time-shift agreed with those obtained from the infrared image. When the tissue temperature was higher than 45 °C, ultrasound temperature imaging is difficult to describe the behavior of the heat transfer in a homogeneous medium. In this study, we used the experimental setup based on combining ultrasound and infrared systems to confirm the reliability and limitations of ultrasound temperature imaging in RFA monitoring. Such an experimental design may be considered as an indispensable platform for the development and optimization of ultrasound temperature imaging techniques in RFA monitoring. © 2014 The Japan Society of Applied Physics

1. Introduction

Radio frequency ablation (RFA) is a minimally invasive therapeutic alternative modality for liver tumor treatment.[1,2] During the RFA procedure, a radio frequency (RF) needle electrode is inserted into the tumor to deliver a strong alternating electrical current. This current agitates ions and produces a temperature increase that induces the coagulation necrosis of tissues surrounding the electrode. Previous research has proven RFA to be a reliable method for treating tumors.[3] Image guidance to insert the needle electrode to the correct location of the tumor is an indispensable procedure during RFA treatment. Among the various medical imaging techniques, ultrasound B-mode imaging is the most commonly used method of guiding RFA. The popularity of B-mode imaging in RFA guidance is based on its portability, low cost, real-time capability, and compatibility with other medical equipment.[4–6]

During RFA treatment, temperature monitoring is essential for quantifying the thermal dosage for better treatment control. Ultrasound techniques can also be simultaneously used to image the temperature distribution in tissues. This is because a change in temperature affects the properties of the scattering medium, thereby altering the acoustic properties of ultrasound propagation, including sound speed,[7,8] attenuation,[9,10] and backscattered energy.[11–13] Among all methods, the echo time-shift that results from a change in the sound speed and tissue thermal expansion has received considerable attention in the last decade.[14–16] Previous studies have successfully applied ultrasound temperature imaging based on echo time-shift detection to monitor RFA.[17,18]

To evaluate the reliability of visualizing the RFA-induced temperature distribution in tissues by ultrasound, a calibration method is necessary when developing the algorithm and computational procedures of ultrasound temperature imaging. In reference to other studies, the use of thermocouples to measure temperatures at different locations in tissues is the most frequently used method of calibration.[17–19] The main limitation of their use is that a practical temperature map of tissues is not available for comparison with ultrasound temperature imaging. To resolve this problem, the region of tissue necrosis induced by thermal ablation may be used as a standard reference for comparison with the temperature image. However, the region of tissue necrosis depends on temperature and needs to correlate with the ablation time. In the early stage of ablation, the region of tissue necrosis may not be well developed owing to the lack of sufficient thermal doses. For this reason, use of the necrosis region to evaluate the overall reliability of ultrasound temperature imaging during RFA is not a good option.

To date, no evidence is available that demonstrates that the temperature distribution detected by ultrasound matches the practical temperature profile in tissues. To clarify the correlation between ultrasound temperature imaging and the practical temperature distribution in tissues, in this study, we designed an experimental setup to compare ultrasound temperature imaging with infrared imaging, which is used as a standard temperature map. The results showed that the temperature distribution measured by ultrasound corresponds well to that obtained from infrared imaging, meaning that ultrasound temperature imaging is a reliable tool for visualizing the practical temperature map.

---

†These authors contributed equally to this work.
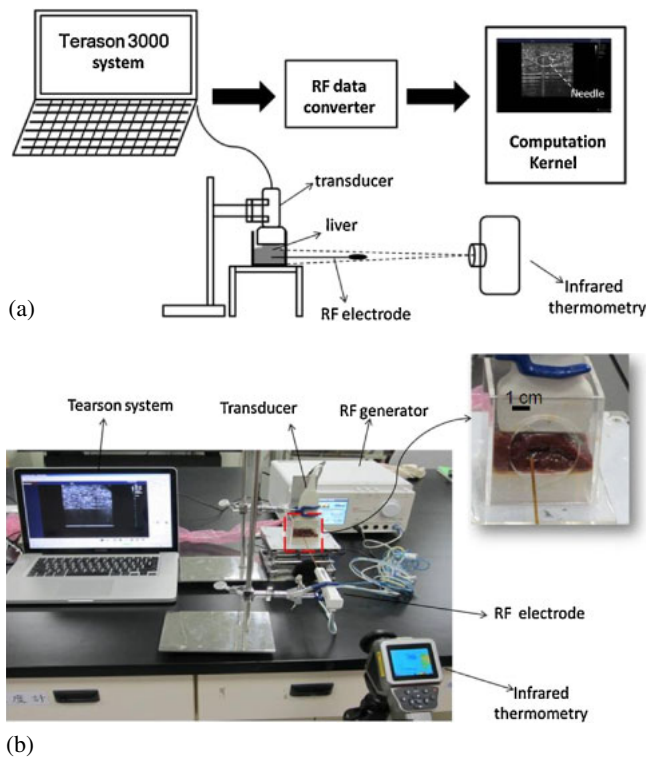
Fig. 1. (Color online) Experimental setup of RFA and monitoring systems, including an ultrasound scanner and an infrared imaging system. (a) Schematic diagram of experimental setup, (b) practical measurement environment and arrangements.

2. Materials and methods

2.1 Experimental setup

Figure 1 illustrates the experimental platform and method proposed to validate the reliability of ultrasound temperature imaging in monitoring RFA. The experimental setup consists of three main systems and accessories: a radio frequency system, an ultrasound imaging scanner, an infrared imaging system, and a tissue sample holder. The RFA system (Starmed VIVA RF generator) used to ablate the tissue in the experiments consists of a needle electrode of 1.5 cm length (Starmed 17-20V15-40), an RF generator, cables, and other accessories. The operation frequency of RFA is 480 kHz. A commercial ultrasound scanner (Terason 3000) equipped with a 7.5 MHz linear array transducer (Terason 10L5) was used to acquire image raw backscattered data from tissues during RFA. An infrared camera (Sunrite Technology DL770A) was placed in front of the tissue sample to monitor the surface temperature map in a tissue.

Five porcine livers ($n = 5$) with dimensions of about 6 (width) × 4 (height) × 3 (thickness) cm^3 obtained from local markets were used as test samples. The liver sample was placed in an acrylic case. One side of the acrylic case facing the infrared camera had a hole with a diameter of approximately 4 cm so that the cross section of the liver sample can be directly exposed to the infrared radiation. For each liver sample, only the first half of the RFA electrode (corresponding to a length of 0.75 cm) was inserted into the tissue. Such an arrangement allows the heat induced by RFA to spread to the cross section of the tissue sample for infrared imaging. Subsequently, the power and duration of RFA were

set at 10 W and 3 min, respectively. During RFA, the infrared imaging system was enabled to monitor the surface temperature map corresponding to the cross section of the tissue. Meanwhile, the ultrasound transducer was placed near the cross section of the tissue sample as closely as possible to acquire backscattered data of the ultrasound image at a sampling rate of 30 MHz. This step allows the acquired image raw data to correspond to the tissue cross section for comparison with the practical temperature map obtained from the infrared system.

2.2 Infrared thermometry

The infrared camera is a device that forms an image using infrared radiation. In general, objects at room temperature emit mainly in the far-infrared region of the wavelength spectrum, but as the temperature rises, the emission appears in the infrared and, finally, in the visible spectrum. The Stefan–Boltzmann law states that the total energy radiated per unit surface area of a black body across all wavelengths per unit time, I, is directly proportional to the fourth power of the black body's thermodynamic temperature T:

$$I = \sigma T^4, \qquad (1)$$

where σ is the Stefan–Boltzmann constant. The total infrared radiation emitted from a general body at temperature T can be modeled by[20]

$$I = \varepsilon \sigma T^4, \qquad (2)$$

where ε is the emissivity. The emissivity is 1 for a black body and is smaller than 1 for a gray body. A liver sample may be similar to a black body radiator because its emissivity is larger than 0.9.[21]

Note that the wavelengths of the used infrared range from 8 to 14 μm, limiting the camera system to detect only the surface temperature without internal temperature information. The infrared system has been calibrated using a black body radiation source by the manufacturer, and therefore, the system can provide reliable temperature measurements. However, the infrared light may be absorbed, scattered, and refracted by air to cause the attenuation effect. Partial heat induced by RFA may also dissipate from the tissue surface. It is difficult to estimate the effects of attenuation and heat dissipation, but these effects indeed cause the bias of temperature measurement to some degree. To reduce errors of measurements on the surface temperature of the tissue, the RF electrode was inserted into the tissue perpendicularly, and the direction for the line of sight between the infrared detector and the tissue surface was adjusted according to the orientation of the RF electrode (Fig. 1). In this arrangement, the RF electrode may still locally appear in the infrared images, but this does not affect the measurements of the surface temperature profile because the temperature of the electrode remains at room temperature during RFA. The alternating electrical current generated by RFA only agitates ions and produces a temperature increase in tissues.

2.3 Ultrasound temperature imaging

The ultrasound backscattered signals were used for B-mode and temperature imaging. The details of the algorithm for ultrasound temperature imaging based on echo time-shift

estimation were described and discussed previously.[22] Here, we briefly explain the principle and assumptions. When ultrasound waves propagate through biological soft tissues, the sound speed is a function of the tissue temperature. Changes in the sound speed in a tissue will produce echo time-shifts for ultrasound backscattered signals. The relationship between temperature change $\Delta T(z)$ and time delay $\delta t(z)$ could be derived as[22]

$$\Delta T(z) = \frac{c_0(z)}{2} \frac{1}{\alpha(z) - \beta(z)} \frac{\partial}{\partial z}(\delta t(z)), \qquad (3)$$

where z is the axial depth along the direction of ultrasound travel, α is the linear coefficient of thermal expansion, β is the thermal coefficient of sound speed, and $c_0(z)$ is the depth-dependent initial sound speed. To simplify the analysis, the following assumptions are made: (i) there was no change in the properties of tissues during increasing temperature (e.g., coagulation); (ii) the material parameter α remains the same within the tissue. The above two assumptions could be satisfied within the temperature range analyzed in this study, and thus, the nonlinear effects associated with thermal expansion could be neglected.[23] Under these assumptions, Eq. (3) could be simplified to

$$\Delta T(z) = k(z) \frac{c_0(z)}{2} \frac{\partial}{\partial z}(\delta t(z)), \qquad (4)$$

where

$$k(z) = \frac{1}{\alpha(z) - \beta(z)} \approx k, \qquad (5)$$

where k is a material-dependent coefficient. Equations (4) and (5) show that the temperature distribution can be estimated by tracking the cumulative echo time-shifts relative to the reference image at each location, and, then, differentiating along the axial direction.[15,22]

By attaching a thermocouple to the tip of the RF electrode to measure the tissue temperature at the electrode location (x_e, y_e), the coefficient k of in vitro porcine liver tissues could be estimated using Eqs. (4) and (5):

$$k \approx \frac{2\Delta T(y_e)}{c_0 \frac{\partial}{\partial y}(\delta t(y_e))}, \qquad (6)$$

where the sound speed c_0 is assumed to be 1540 m/s, $\Delta T(y_e)$ and $(\partial/\partial y)(\delta t(y_e))$ are the temperature change and the differential of echo time-shift with respect to (x_e, y_e) at a specific time of heating, respectively. With Eq. (6), the tissue coefficients k at different temperatures were estimated and used in the temperature estimation.

The algorithm of ultrasound temperature imaging used in this study is implemented according to the following steps. At first, the image raw data at initial reference temperature $r(x, y, t_0)$ prior to RFA heating were acquired. For each time point i during RFA, the incremental time-shift map $\delta \hat{t}_{incr}(x, y, t_i)$ was estimated using the current image data $r(x, y, t_i)$ and the previous one $r(x, y, t_{i-1})$ for one-dimensional cross-correlation analysis. The cumulative echo time-shift map was computed as

$$\delta \hat{t}(x, y, t_i) = \sum_{j=1}^{i} \delta \hat{t}_{incr}(x, y, t_j). \qquad (7)$$

It is necessary to carry out smoothing along both axial and lateral directions to reduce the ripple in the temperature estimates.[22] For this reason, the cumulative echo time-shift map was further filtered using an 8-order low-pass Butterworth filter with normalized cutoff frequency of 0.33, which was obtained empirically in our tests to work well with the experimental system. Finally, the ultrasound temperature image was obtained by differentiating the cumulative echo time-shift map along the axial direction and scaling the result using Eq. (4).

2.4 Data analysis

The temperature curve as a function of ablation time was measured from the temperature values at the electrode location in the infrared images for comparison with ultrasound temperature images. The -6 dB temperature distribution areas obtained from the ultrasound and infrared systems were compared. Data were expressed as mean $\pm$ standard deviation.

3. Results

Figure 2 shows the typical B-mode images of the porcine liver sample acquired in the ablation period. The white arrow in the figure indicates the location of the RF electrode. Figure 3 shows the ultrasound temperature images constructed using the echo time-shift corresponding to the B-scans in Fig. 2. The regions indicated by white lines mean -6 dB temperature distribution areas. The infrared images at various ablation times are shown in Fig. 4. The black circles in the infrared images represent -6 dB areas of temperature distribution, indicating that RFA induced a temperature distribution in the tissue. The temperature values at the electrode location in the infrared images were used to calculate the temperature as a function of the ablation time, as shown in Fig. 5. As the ablation time increases, the temperature increases from approximately 21 to 52 °C. Figure 6 shows the cross section of the liver tissue after RFA ablation. Tissue necrosis can be observed on the tissue cross section, meaning that the RFA-induced temperature distribution satisfied the thermal dose requirement to produce the effect of tissue denaturation. Figure 7 compares the temperatures at the location of the RF electrode measured from ultrasound and infrared images, indicating that the echo time-shift method has a good ability to estimate the temperature variation. In particular, Fig. 8 shows that the -6 dB area of the temperature distribution measured from the ultrasound temperature image is in good agreement with that obtained from the infrared image. In the temperature range between 21 and 45 °C, the -6 dB areas of the temperature distributions estimated from ultrasound and infrared images increased from 0.2 to 1.6 cm^2. However, the area of the temperature distribution detected by ultrasound tends to be underestimated compared with that in the infrared image when the temperature exceeds approximately 45 °C.

4. Discussion

It is well known that ultrasound temperature imaging based on echo time-shift detection can visualize the temperature distribution in a tissue.[15,22–24] The limitations of the echo time-shift method have also been discussed in the literature. Previous research has shown that the sound speed does
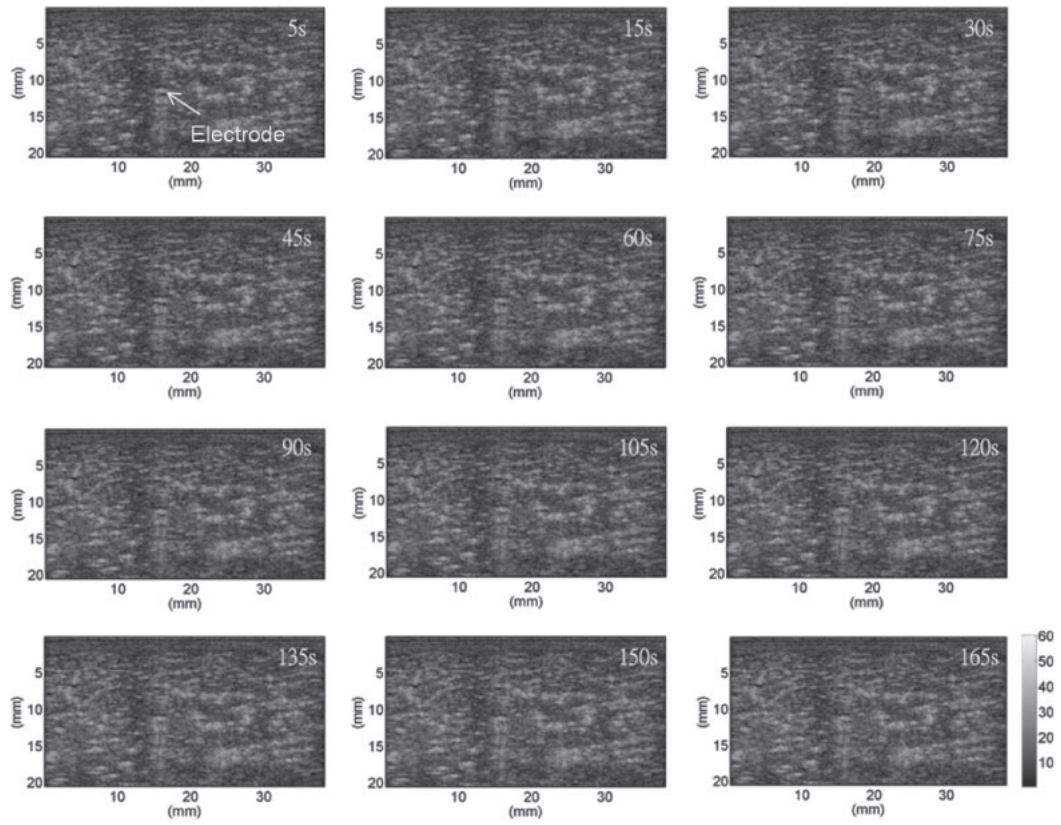
Fig. 2. B-mode images of liver sample acquired at various times during ablation. The white arrow indicates the location of the RF electrode.
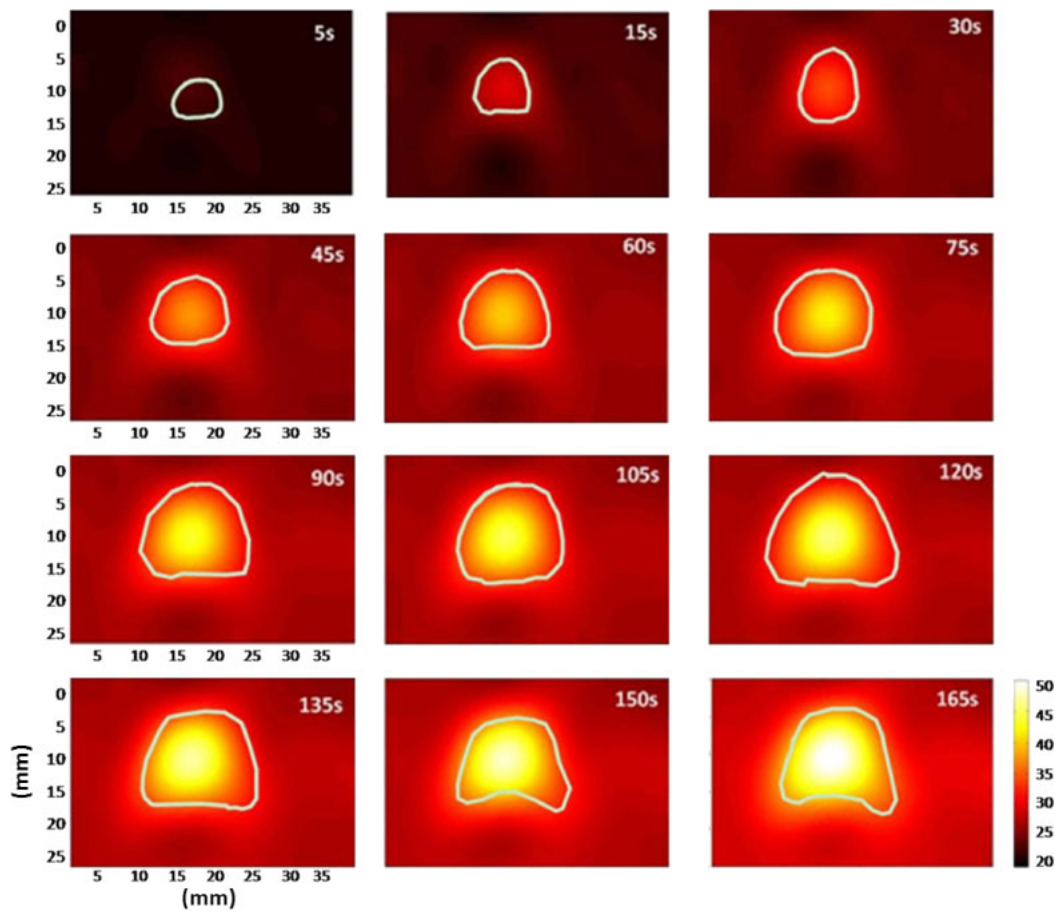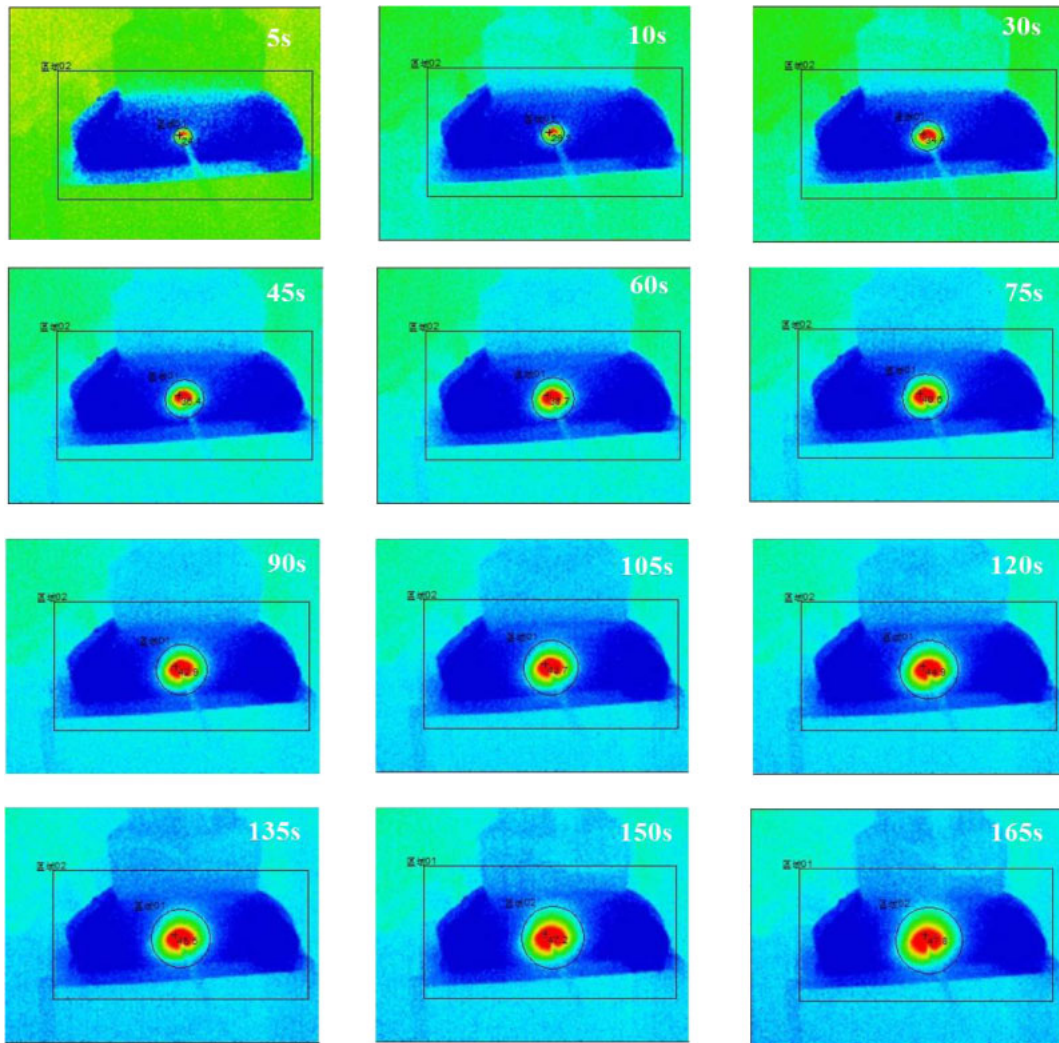

Fig. 3. (Color online) Ultrasound temperature images based on echo time-shift estimation of liver sample acquired at the various ablation times. The white lines represent −6 dB areas of temperature distribution.

Fig. 4. (Color online) Infrared temperature maps corresponding to ultrasound temperature images in Fig. 3. The black circles in the infrared images represent −6 dB areas of temperature distribution.
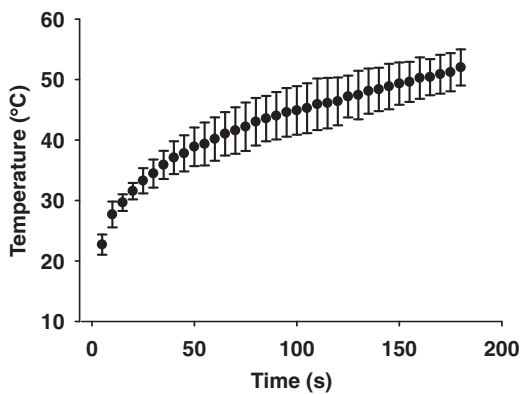
Fig. 5. Average and standard deviation of temperature at location of RF electrode as a function of ablation time.
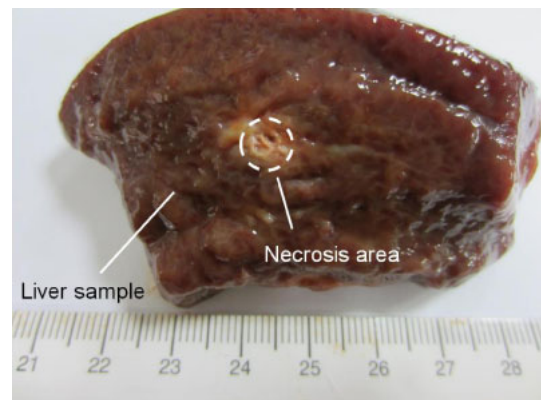
Fig. 6. (Color online) A typical cross section of ablated tissues. The white circle indicates the ablated region. The tissue necrosis induced by RFA can be observed.

not increase significantly at temperatures over 50 °C.[23] In particular, the sound speed of fatty tissues decreases with increases in temperature. Examples of the temperature dependence of the sound speed, such as for breast or fatty liver, can be found in the cited reference,[23] which indicated the difficulty of using echo time-shift to establish the temperature distributions of fatty tissues. For temperature

elevations much higher than 50 °C, the major limitation comes from the irreversible changes in the acoustic properties of tissues caused by necrosis. In the case of coagulative necrosis, the properties of scatterers (e.g., echogenicity, spacing, or arrangement) are completely altered, to make the waveforms of the backscattered signals different from those
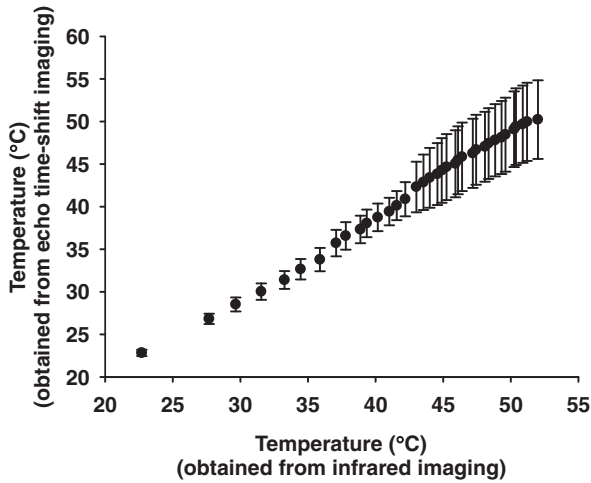
Fig. 7. Comparison of temperatures at location of RF electrode measured from ultrasound and infrared images.
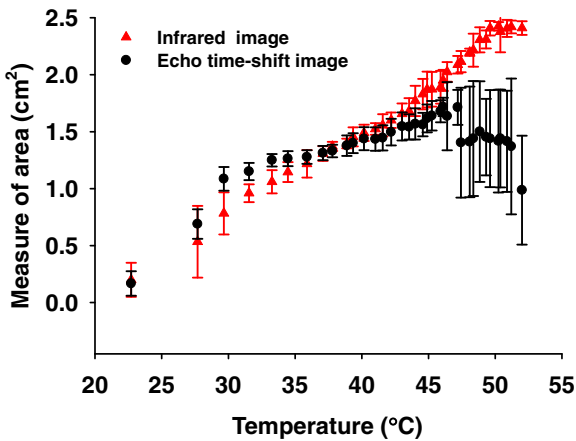

Fig. 8. (Color online) Comparison of −6 dB areas of temperature distribution measured from ultrasound and infrared images. The area of the temperature distribution detected by ultrasound tends to be underestimated compared with that in the infrared image when the temperature exceeds approximately 45 °C.

before ablation (signal decorrelation effect). In this case, the cross-correlation analysis using the backscattered signals acquired before and after heating for tracking echolocation shifts becomes difficult.[25] Moreover, the echo time-shift estimation using the cross-correlation algorithm is sensitive to the tissue motion and bubble formation during RFA, which leads to severe decorrelation between measurements.[26] A high-temperature ablation can also generate cavitation, which results in significant nonlinear aftereffects to cause echo distortions. The effects of bubbles on the measured echo time-shift depend on how they affect the phase characteristics of the echo signals.[7]

In this study, we found that the temperature estimated from ultrasound echo time-shift highly correlates with measurements from the use of infrared imaging. There is a good consistency between the areas of temperature distribution measured using ultrasound echo time-shift and infrared imaging. The evidence provided by the infrared image indicates that the ultrasound temperature image is a reliable approach in the visualization of temperature distribution. Meanwhile, the use

of infrared imaging in the experimental design also pointed out the dilemma of ultrasound temperature imaging. Evidently, the estimation bias of the temperature distribution is significant when the temperature exceeds 45 °C.

Using the experimental setup, we further observed some problems of ultrasound temperature imaging in visualizing the practical temperature distribution in a tissue. According to the results of the infrared images, the practical temperature distribution in a tissue induced by RFA behaves in a circular shape. This is reasonable because the liver is essentially a homogeneous tissue. A previous study has demonstrated that heat transfer in a homogeneous medium forms a temperature distribution with a circular shape.[27] However, when the temperature exceeds 45 °C, the circular pattern of the heat transfer in a homogeneous medium cannot be well described by ultrasound temperature imaging. Possible reasons why the echo time-shift cannot accurately describe the practical shape of the temperature distribution in a tissue may include the imperfection of algorithms and system factors. It has been shown that echo time-shift estimation is highly dependent on the filter design for the reduction of artifacts (e.g., thermal lens effect).[15,22] Furthermore, the sampling rate of 30 MHz for the ultrasound system used in this study may not be sufficient to describe the echo time-shift in more detail.

Here, we want to emphasize that the experimental setup based on the combination of an ultrasound scanner and the infrared imaging system provides us a direct and effective platform to allow real-time observation of the heat diffusion during RFA and the comparison of ultrasound temperature imaging with the practical temperature map in the tissue. Under a condition that many algorithmic and system factors need to be taken into account in practice, the proposed experimental method can serve as a standard calibration platform to optimize the algorithms and system settings for ultrasound temperature imaging.

Some considerations when using the proposed experimental method in practical applications need to be discussed here. First, the experimental method is useful for the calibration of ultrasound temperature imaging for correctly visualizing the heat transfer pattern and the temperature distribution in a tissue. However, it should be noted that a difference in size between the temperature maps measured using ultrasound and infrared images may exist, because both ultrasound and infrared imaging are impossible to carry out in the same plane. To reduce measurement errors, operators must adjust the position of the ultrasound transducer to approximate the frame of ultrasound imaging to the cross section of the tissue. Second, the proposed experimental method is only suitable for use in developing ultrasound temperature imaging techniques dedicated to RFA or microwave ablation monitoring. Thermal ablation using high-intensity focused ultrasound (HIFU) needs water or gel for acoustic coupling, and thus, the reliability of ultrasound temperature imaging used to monitor HIFU is typically validated by egg white phantoms.[28]

5. Conclusions

This is the first study to use infrared images for evaluating the reliability of using ultrasound temperature imaging to visualize the practical temperature map in a tissue. According to the lines of evidence provided by infrared imaging, we

found that the range of the temperature distribution estimated from the ultrasound echo time-shift is consistent with that measured from the infrared image when the tissue temperature is smaller than 45 °C. However, the typical pattern of the heat transfer (circular-shape distribution) in a homogeneous medium cannot be well described by ultrasound temperature imaging as the tissue temperature continues to increase to satisfy the thermal dosage required to cause tissue necrosis. It is worth mentioning that the experimental method based on combining ultrasound and infrared systems allows real-time observations and demonstrations of the strengths and weaknesses of ultrasound temperature imaging. Such an experimental design may be further considered as an indispensable platform for the development and optimization of ultrasound temperature imaging techniques in RFA monitoring.

Acknowledgements

1) H. B. El-Serag, J. A. Marrero, L. Rudolph, and K. R. Reddy, Gastroenterology **134**, 1752 (2008).
2) R. Lencioni and L. Crocetti, Tech. Vasc. Interv. Radiol. **10**, 38 (2007).
3) S. N. Goldberg, Eur. J. Ultrasound **13**, 129 (2001).
4) S. Y. Chiou, J. B. Liu, and L. Needleman, J. Ultrasound Med. **26**, 487 (2007).
5) L. Solbiati, T. Ierace, M. Tonolini, and L. Cova, Eur. J. Radiol. **51**, S19 (2004).
6) J. Machi, S. Uchida, K. Sumida, W. M. L. Limm, S. A. Hundahl, A. J. Oishi, N. L. Furumoto, and R. H. Oishi, J. Gastrointest. Surg. **5**, 477 (2001).
7) R. Maass-Moreno and C. A. Damianou, J. Acoust. Soc. Am. **100**, 2514 (1996).
8) R. Maass-Moreno, C. A. Damianou, and N. T. Sanghvi, J. Acoust. Soc. Am. **100**, 2522 (1996).
9) C. A. Damianou, N. T. Sanghvi, F. J. Fry, and R. Maass-Moreno, J. Acoust. Soc. Am. **102**, 628 (1997).
10) P. D. Tyréus and C. Diederich, Phys. Med. Biol. **49**, 533 (2004).
11) W. L. Straube and R. M. Arthur, Ultrasound Med. Biol. **20**, 915 (1994).
12) R. M. Arthur, W. L. Straube, J. D. Starman, and E. G. Moros, Med. Phys. **30**, 1021 (2003).
13) R. M. Arthur, W. L. Straube, J. W. Trobaugh, and E. G. Moros, Int. J. Hyperthermia **21**, 589 (2005).
14) M. D. Abolhassani, A. Norouzy, A. Takavar, and H. Ghanaati, J. Ultrasound Med. **26**, 215 (2007).
15) D. Liu and E. S. Ebbini, IEEE Trans. Biomed. Eng. **57**, 12 (2010).
16) A. M. Pouch, T. W. Cary, S. M. Schultz, and C. M. Sehgal, J. Ultrasound Med. **29**, 1595 (2010).
17) M. J. Daniels, T. Varghese, E. L. Madsen, and J. A. Zagzebski, Phys. Med. Biol. **52**, 4827 (2007).
18) M. J. Daniels and T. Varghese, Phys. Med. Biol. **55**, 4735 (2010).
19) T. D. Mast, D. P. Pucke, S. E. Subramanian, W. J. Bowlus, S. M. Rudich, and J. F. Buell, J. Ultrasound Med. **27**, 1685 (2008).
20) J. Enderle, S. Blanchard, and J. Bronzino, *Introduction to Biomedical Engineering* (Academic Press, Burlington, MA, 2005).
21) G. J. Müller and A. Roggan, *Laser-induced Interstitial Thermotherapy* (SPIE Press, Bellingham, WA, 1995).
22) C. Simon, P. VanBaren, and E. S. Ebbini, IEEE Trans. Ultrason. Ferroelectr. Freq. Control **45**, 1088 (1998).
23) N. R. Miller, J. C. Bamber, and P. M. Meaney, Ultrasound Med. Biol. **28**, 1319 (2002).
24) T. Varghese, J. A. Zagzebski, Q. Chen, U. Techavipoo, G. Frank, C. Johnson, A. Wright, and F. T. Lee, Jr., Ultrasound Med. Biol. **28**, 321 (2002).
25) M. Pernot, M. Tanter, J. Bercoff, K. R. Waters, and M. Fink, IEEE Trans. Ultrason. Ferroelectr. Freq. Control **51**, 606 (2004).
26) I. Winkler and D. Adam, Ultrasound Med. Biol. **37**, 755 (2011).
27) M. J. Daniels, J. Jiang, and T. Varghese, Ultrasonics **48**, 40 (2008).
28) K. Takegami, Y. Kaneko, T. Watanabe, T. Maruyama, Y. Matsumoto, and H. Nagawa, Ultrasound Med. Biol. **30**, 1419 (2004).